Chapter 1

Biomedical Applications of Materials Processed in Glow Discharge Plasma

V. Tereshko, A. Gorchakov, I. Tereshko, V. Abidzina and V. Red'ko

Additional information is available at the end of the chapter

http://dx.doi.org/10.5772/55548

1. Introduction

There is exhaustive literature about interactions of charged particles with solid surfaces [l, 2]. For a long period only high energies were assumed to cause any significant modifications. However, low-energy ion bombardments (up to 5 keV) of metal and alloy samples were shown to be very efficient too: the increase of dislocation density (up to 10 mm in depth from the irradiated surface) was detected [3–7]. In fact, a bulk long-range modification of materials in the glow discharge plasma (GDP) took place. The above results were obtained by the use of transmission electron microscopy for well annealed samples with initially small dislocation density (armco-Fe, Ni3Fe, *etc*.) [4, 6]. For materials with initially increased dislocation density (unannealed copper, M2 high-speed steel, titanium alloys) reorganization of dislocation structure is the most considerable: either intensive formation of the dislocation fragments or grinding of the fragments with corresponding increase in their disorientation is observed. These reorganizations also take place well below the irradiated surface. When the ion energy decreases by 1 keV, the modified layer became even deeper [7].

The above results can only be explained by taking the nonlinear nature of atom interactions into account. The ion bombardment is assumed to induce nonlinear oscillations in crystal lattices leading to self-organization of the latter. Modelling shows the formation of new collective atom states. The observed phenomena include the redistribution of energy, clusterization, structure formation when the atoms stabilizes in new non-equilibrium positions, localized structures, auto-oscillations, and travelling waves and pulses [3–7].

The next step was to look at the influence of low-energy GDP on liquids. Water that occupies up 70 percent of the Earth's surface and is the main component of all living things

was taken for investigation. Water molecules are able to create molecular associates using Van der Waals forces as well as labile hydrogen interactions [8–11]. Owing to hydrogen bonds molecules of water are capable to form not only random associates (one having no ordered structure) but clusters, i.e. associates having some ordered structure [9–11]. The network of hydrogen bonds and the high order of intermolecular cooperativity facilitate long-range propagation of molecular excitations [12, 13]. This allows, in principle, to consider water and water-based solutions as systems sensitive to weak external forces. Indeed, the study of luminescence at long time scale shows that the structural equilibrium in water is not stable: it changes after dissolution of small portions of added substances and after exposition of aqueous samples to UV and mild X-ray irradiation [14].

The results obtained by Lobyshev, *et al* opened up the new avenues to water and aqueous solutions as non-equilibrium systems capable of self-organization [14]. The key property of self-organization is, however, nonlinearity to which, in models of water, hasn't paid the required attention yet. The present paper is aimed to cover this flaw. Basic models of nonlinear chains that can be related to water structure were investigated. We observed self-organization processes resulting in the displacement of atoms and their stabilization in new positions, which can be viewed as the formation of water clusters.

In experiments, we exposed crop seeds, baking yeast and water to GDP. The results were very promising: the seed sprouts showed greater growth and the yeast showed greater metabolic activity compared to the control samples. The results on volunteers with different diseases, who either drunk the processed water or was injected intravenously with the processed physiological solution, were encouraging too. The diagnostics of volunteers' blood immune cells (lymphocytes and leukocytes) showed significant normalization of their state toward homeostasis.

Next part of this paper is devoted to the study of properties of implants processed in GDP. The modern medicine is characterized by active introduction of high technologies to clinical practice. It requires sufficient biocompatibility of implanted mechanical, electromechanical and electronic devices with natural tissues. The properties of materials are crucial, since insufficient biocompatibility can lead to the negative reactions to the implant from the side of surrounding tissues causing inflammatory processes, dysfunction of the endothelium, disturbance of homeostasis, destruction and the necrosis of bone tissue and so forth [15, 16]. The formation of hydrophilic coatings and the modification of chemical composition and topography of the implant surface make it possible to reduce the frequency of the development of negative processes. The bone, fibrous and endothelial tissues are uniquely structured, and the attempts to design the next generations of implants are focused on the development of unique nanotopography of the surface of implants based on the imitation of nature. Our and other studies showed the effectiveness of vacuum-plasma technology for improving biocompatibility and durability (mechanical and chemical) of implanted materials [17–19]. New avenues in the application of above technology to the titanium implants and their influence to surrounding tissues are explored in this paper.

http://dx.doi.org/10.5772/55548

2. Modelling atomic and molecular chains

Molecular dynamics were used to develop the model. To describe the atomic and molecular interactions, Morse (1) and Born-Mayer (2) potentials were chosen [2].

Morse potential takes the form

$$U(r) = J\left\langle \exp\left[-2\alpha\left(r - r_0\right)\right] - 2\exp\left[-\alpha\left(r - r_0\right)\right]\right\rangle \tag{1}$$

where J and α are the parameters of dissociation energy and anharmonicity respectively; $\Delta r = \left(r - r_0\right)$ is the displacement from an equilibrium.

Born-Mayer potential takes the form

$$U(r) = T \cdot e^{\frac{-r}{a}} \tag{2}$$

where T, a, and r are the energy constant, the shielding and atomic lengths respectively.

We assume the existence of multiple equilibria corresponding to thermodynamic as well non-thermodynamic branches. Expanding the potentials in a Taylor series (up to the fifth order term), find the interaction force

$$F = -\frac{dU\left(r\right)}{dr} = -K\Delta r + A\Delta r^2 - B\Delta r^3 + C\Delta r^4 - D\Delta r^5 \tag{3}$$

For the Morse potential

$$\begin{aligned} &K = 2\alpha^2 J,\ A = 3\alpha^3 J,\ B = 2.3\alpha^4 J, \\ &C = 1.25\alpha^5 J,\ D = 1.1\alpha^6 J \end{aligned} \tag{4}$$

where K, A, B, C, D are the coefficients of elasticity, quadratic cubic, fourth and fifth orders nonlinearities respectively.

For the Born-Mayer potential

$$K = \frac{T}{a^2},\quad A = \frac{T}{2a^2},\quad B = \frac{T}{6a^4},\quad C = \frac{T}{24a^5},\quad D = \frac{T}{120a^6}. \tag{5}$$

The coefficient values are presented in Table 1.

Coefficient	Born-Mayer potential	Morse potential
K, N/m	$9{,}341 \bullet 10^{4}$	$1{,}140 \bullet 10^{4}$
A, N/m^2	$1{,}951 \bullet 10^{15}$	$8{,}244 \bullet 10^{14}$
B, N/m^3	$2{,}716 \bullet 10^{25}$	$3{,}046 \bullet 10^{25}$
C, N/m^4	$2{,}836 \bullet 10^{35}$	$7{,}980 \bullet 10^{35}$
D, N/m^5	$2{,}370 \bullet 10^{445}$	$3{,}385 \bullet 10^{446}$

Table 1. Coefficients for Morse and Born-Mayer potentials.

There are many models that describe water molecules [13]. The molecular structure of water is presented in Figure 1. The covalent and hydrogen bonds are marked by the grey springs and the bold lines respectively. For simplicity, in our simulations we consider a chain, i.e. 1D lattice, of water molecules (see the marked area of Figure 1).

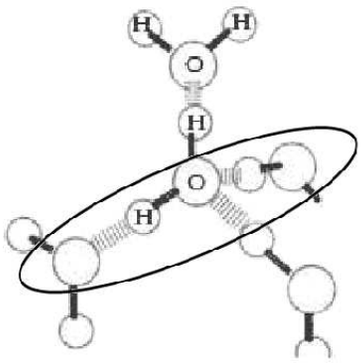

Figure 1. Molecular structure of water in a solid phase. The ellipse marks a piece of 1D chain used in simulations.

Considering only single component of $r = (x, y, z)$, say x, and viewing the atom as interacting nonlinear oscillators, the system equations take the form:

$$
\begin{aligned}
&m\frac{d^2x_1}{dt^2} = -K'x_1 + Ax_1^2 - Bx_1^3 + Cx_1^4 - Dx_1^5 + K\left(x_2 - x_1\right) - \\
&-A\left(x_2 - x_1\right)^2 + B\left(x_2 - x_1\right)^3 - C\left(x_2 - x_1\right)^4 + D\left(x_2 - x_1\right)^5 - \beta'\frac{dx_1}{dt}, \\
&m\frac{d^2x_i}{dt^2} = -K\left(x_i - x_{i-1}\right) + A\left(x_i - x_{i-1}\right)^2 - B\left(x_i - x_{i-1}\right)^3 + C\left(x_i - x_{i-1}\right)^4 - \\
&-D\left(x_i - x_{i-1}\right)^5 + K\left(x_{i+1} - x_i\right) - A\left(x_{i+1} - x_i\right)^2 + B\left(x_{i+1} - x_i\right)^3 - C\left(x_{i+1} - x_i\right)^4 + \\
&+D\left(x_{i+1} - x_i\right)^5 - \beta\frac{dx_i}{dt}, \\
&m\frac{d^2x_n}{dt^2} = -K\left(x_n - x_{n-1}\right) + A\left(x_n - x_{n-1}\right)^2 - B\left(x_n - x_{n-1}\right)^3 + C\left(x_n - x_{n-1}\right)^4 - \\
&-D\left(x_n - x_{n-1}\right)^5 - K'x_n + Ax_n^2 - Bx_n^3 + Cx_n^4 - Dx_n^5 - \beta'\frac{dx_n}{dt},
\end{aligned}
\tag{6}
$$

http://dx.doi.org/10.5772/55548

where x_i, $i = 1,\ldots, n$ is displacement of i-th oscillator from the its equilibrium position, K′ is the coefficient of elasticity on the chain borders, and ß and ß′ are the damping factors inside the chain and on its borders respectively. The system (6) was solved by the Runge–Kutta method.

Relaxation processes of atoms after stopping the external influence were under investigation. Sources that gave impulses to atoms of the chains were both direct ion impact on the first atom of the chain (single impact) and random impacts on randomly chosen atoms of the chain (plasma treatment). In practice the atom bonds are important to keep unbroken, so all types of influences were low-energy ones.

2.1. Hydrogen atom chain

We carried out the simulations for chain consisting of 50 hydrogen atoms (Figure 2). Morse potential was chosen; N_i defines the number of i-th atoms. For single impact the first atom of the chain was displaced with velocity $V = 500$ m/s, which corresponds to 10^{-3} eV of the exposed energy. In case of plasma treatment the following atoms were exposed to low-energy impacts: atom N_1 ($V = 538$ m/s), atom N_{10} ($V = 1682$ m/s) and atom N_{30} ($V = 1237$ m/s).

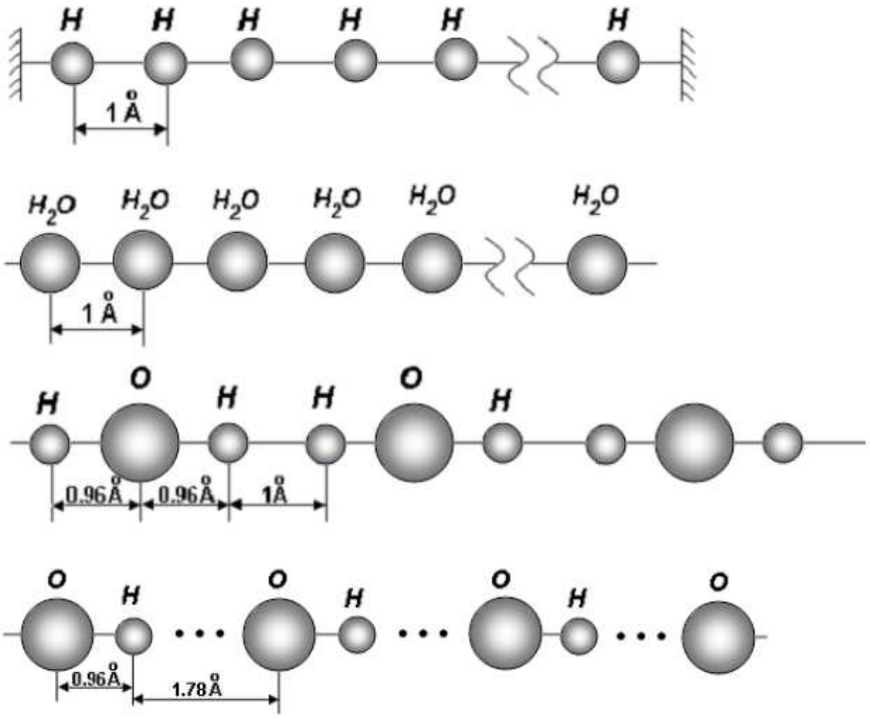

Figure 2. Chain of hydrogen atoms.

Figure 3 illustrates the atom displacements after the plasma treatment. The atoms are stabilized in the new positions that can be described as (nano)clusters (atoms $N_{1\text{--}29}$ and $N_{30\text{--}50}$). After atom relaxation the simulations were continued fourth times longer, and the persistent stabilization was always observed.

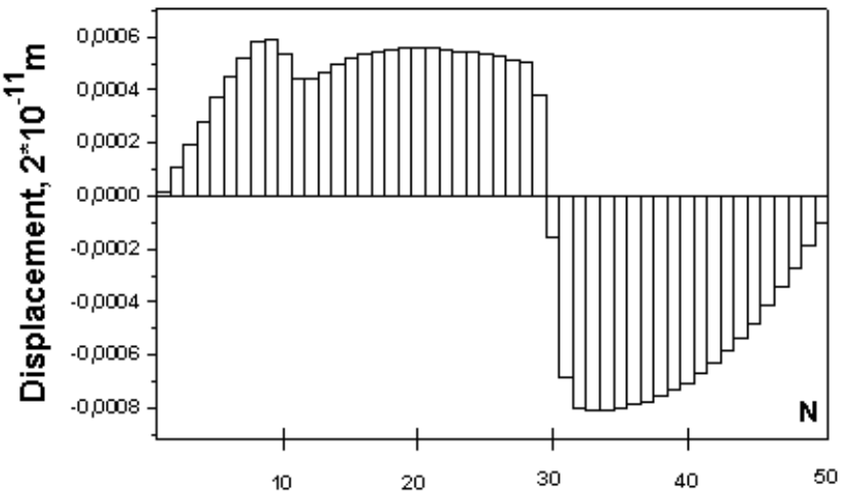

Figure 3. Displacement of 50 atoms of the excited nonlinear chain at the time of stabilization. *N* defines the atom number in the chain.

2.2. H–O–H molecule chain

We investigated the chain of H–O–H molecules shown in Figure 4. From two to eight molecules (6–24 atoms) were used. The equilibrium distances between H and O atoms inside the molecule are 0.96 Å, and the equilibrium distance between the molecules is 1 Å, which corresponds to … Single impact were assumed, and the velocity of the first atom was varied from 100 to 1600 m/s, which corresponds to 10^{-5}–10^{-2} eV of the exposed energy. Again, Morse potential was used.

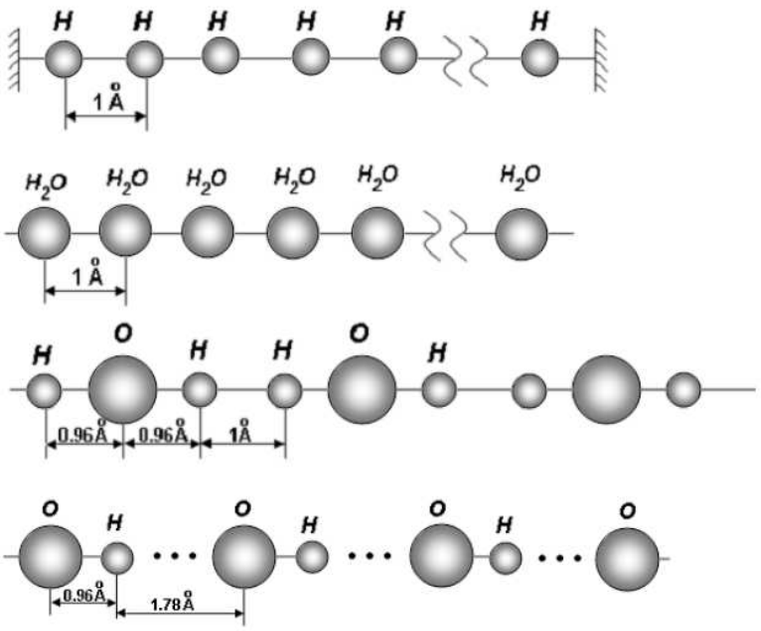

Figure 4. Atom chain of water consisting of hydrogen and oxygen atoms.

http://dx.doi.org/10.5772/55548

Figure 5 illustrates the atom displacements versus the velocity that the first atom received from external impact. In all cases significant shrinkage, or collapse, of the chains is observed. One can see that the length of the collapsed chain depends on the above velocity, the minimal length being detected at some low impact energies. For example, for the chain consisting of eight H–O–H molecules the minimal length of the chain was observed at V = 1200 m/s (see Fig. 5b).

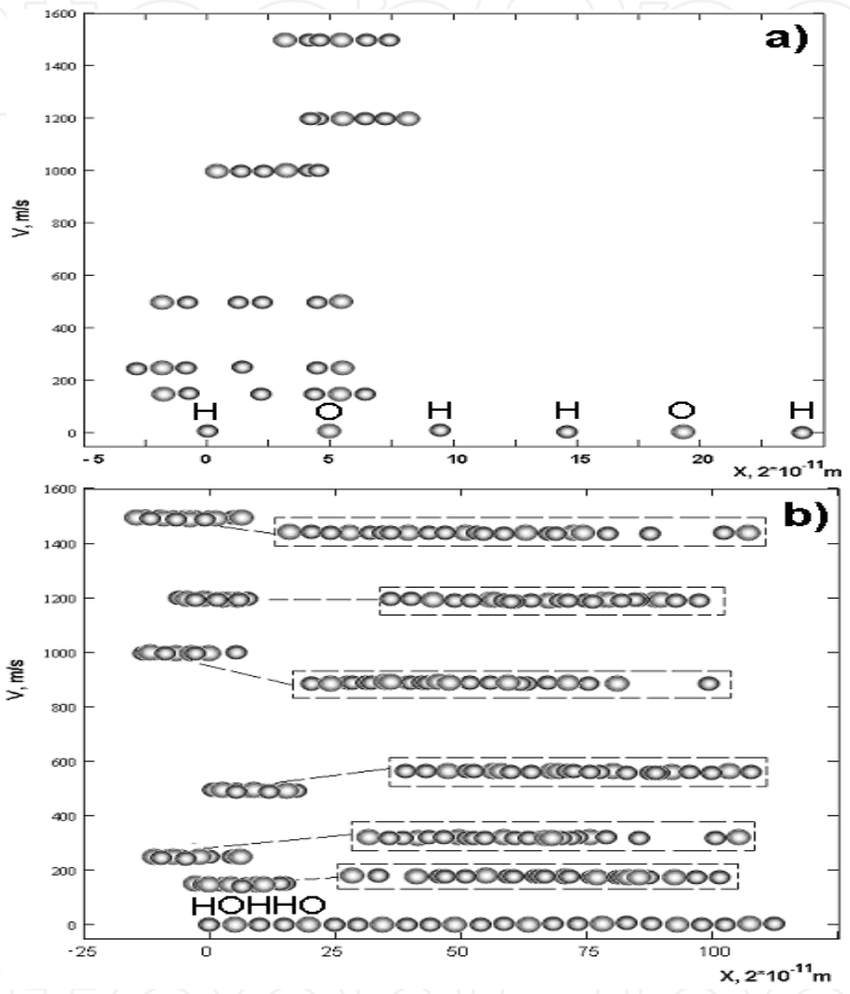

Figure 5. Atom displacements in the chain of H–O–H molecules versus the velocity received by the first atom: a) chain consisting of two molecules, b) chain consisting of eight molecules. In dashed areas the collapsed chains are shown enlarged.

2.3. 1D water molecule chain

Finally, we investigated the chain shown in Figure 6. It corresponds to the 1D cut of water molecule (see the area marked by the ellipse in Figure 1). The solid and dotted lines correspond to the covalent and hydrogen bonds respectively. As one can see the covalent bonds yields the equilibrium between O and H atoms at 0.96 Å whereas the hydrogen bonds yields the equilibrium at about twice longer distance (1.78 Å).

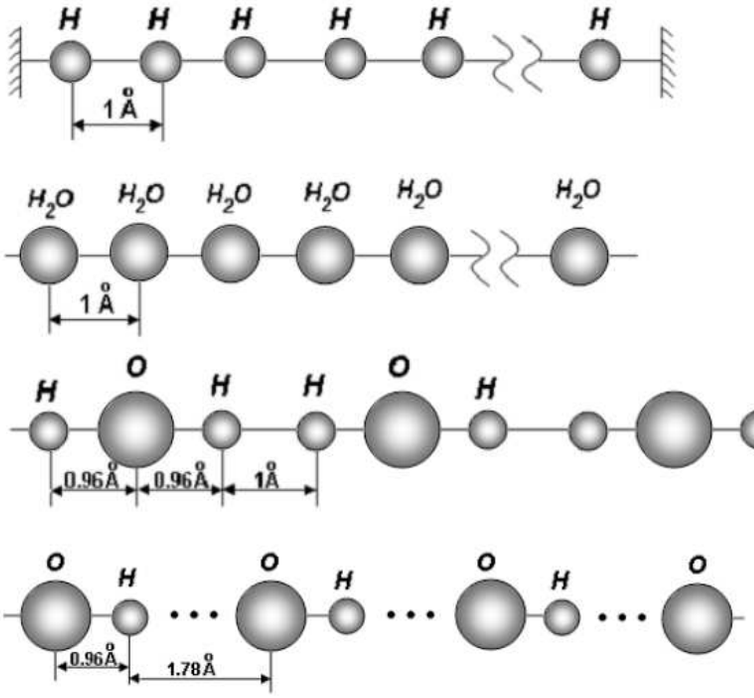

Figure 6. chain of water consisting of hydrogen and oxygen atoms. The solid and dotted lines mark the covalent and hydrogen bonds respectively.

In simulations we considered simple chain consisting of two 1D water molecules. The initial velocity of the first atom was taken at $V = 500$ m/s. The Morse and Born-Mayer potentials were used for this investigation.

Figure 7 represents the initial and final stabilized conditions of atom chains (after direct low-energy ion impact to the first atom of the chain) calculated with Born-Mayer (Figure 7a) and Morse (Figure 7b) potentials

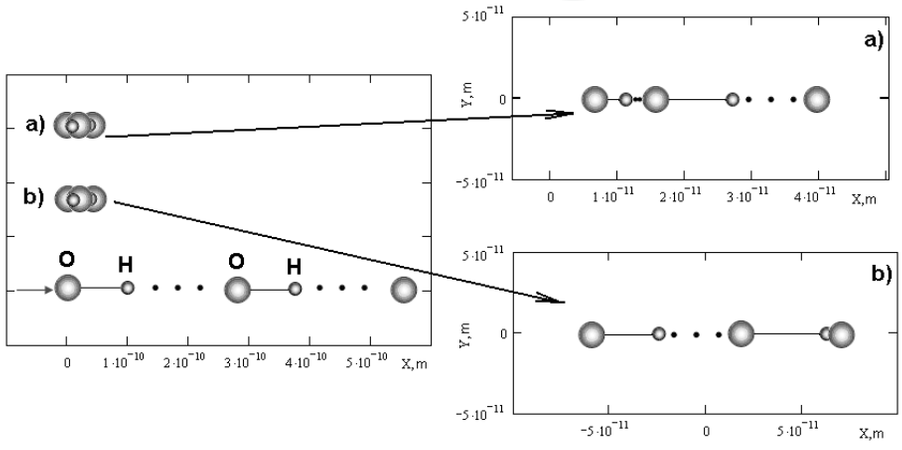

Figure 7. Initial and final positions of atoms of 1D water molecule after direct low-energy impact to the first atom (oxygen): a) Born-Mayer potential, b) Morse potential. The right figures show the enlarged final chains.

http://dx.doi.org/10.5772/55548

3. Biomedical applications

Biological objects are known for their high sensitivity to weak external fields. The evidence that electromagnetic fields can have "non-thermal" biological effects is now overwhelming. When the production of heat shock proteins is triggered electromagnetically it needs 100 million times less energy than when triggered by heat [20]. Low-frequency weak magnetic fields may lead to the resonant change of the rate of biochemical reactions although the impact energy is by ten orders of magnitude less than $k_B T$ where k_B is the Boltzmann constant and T is the temperature of the medium [21].

The therapeutic ability of the low intensity electromagnetic radiations is actively discussed [22]. The low-power millimeter wave irradiation and magnetic-resonance therapy are used in practical medicine already, which differ significantly from the drug treatment by the fact that they do not clog organism with the undesirable chemical compounds, i.e. xenobiotics. In this chapter we discuss the biomedical application of vacuum-plasma technologies.

3.1. Activating and therapeutic properties of water processed in GDP

To understand the above extreme sensitivity of living objects, investigations in influences of weak fields on water appear to be essential. Indeed, water plays a major role in biological processes. A man consumes about 2 l of drinking water a day. Water is the main component of human, animal, plant and generally every living being body. A new-born child body contains 97% of water, decreasing to 70–75% with aging. In particular, human brain consists of about 85% of water.

So, we performed experiments with water, crop seeds and baking yeast *S. cerevisiae*. The crop seeds and yeast were processed directly in GDP. Also, the untreated crop seeds and yeast were poured with the water processed in GDP. In all cases practically the same biotrophic effects were observed. Namely, the seed sprouts showed the growth in 3–4 times higher than the control samples. Both the processed yeast and the unprocessed one that immersed in the processed (by GDP) water showed greater metabolic activity compared to the control samples.

The obtained results allow suggesting that the discovered phenomena can be used for direct correction of pathological states. Therefore we processed water and physiological solution. The samples were exposed to low-energy ion irradiation in GDP of residual gases. The ion energy depends on the voltage in the plasma generator. The latter was kept at 1.2 keV while the current in the plasma generator was maintained at 70 mA. The temperature in the chamber was controlled during the irradiation process and did not exceed 298 K (25° C). The irradiation time was 60 minutes.

In test experiments, volunteers with different diseases either drunk the processed water or they were injected intravenously with the similarly processed physiological solution. The course of treatment included 3–5 sessions of 0.5 l physiological solution transfusion. The preliminary results appeared to be very promising. We were most interested in the therapeutic treatment of the global inflammatory processes such as cardio-vascular diseases and pancre-

atic (insular) diabetes complicated by the acute and chronic forms of atherosclerosis. Also, different types of oncology, say, leukemia, etc., were under investigation.

The blood immune cells were taken for diagnostics. The immune system is known as one of the leading homeostatic systems in the organisms. It may serve as a mirror that reflects practically all adaptations and pathological rearrangements. The immunocompetent cells, lymphocytes and leukocytes, have a set of properties that may be used as an indicator of the organism state. In addition, the structural organization of blood lymphocytes and leukocytes makes possible a most efficient use of microspectral analysis and different fluorescent probes for their studies [23].

We used the dual-wavelength microfluorimetry analysis. The selected cell populations (mono- and polynuclears of blood immunocytes) were mapped as clusters of points on the phase plane in coordinates of the red and green luminescence intensities, i.e. on the wavelengths I_{530} (abscissa) and I_{640} (ordinate). Figure 8 presents the above phase plane for an oncologic outpatient before and after the monthly course treatment. The black and grey pluses represent lymphocyte and leukocyte cells respectively. The white ellipses mark the distribution of fluorescent signals of lymphocytes (lower ellipse) and leukocytes (upper ellipse) in norm. As seen, the treatment results into significant normalization toward the homeostasis.

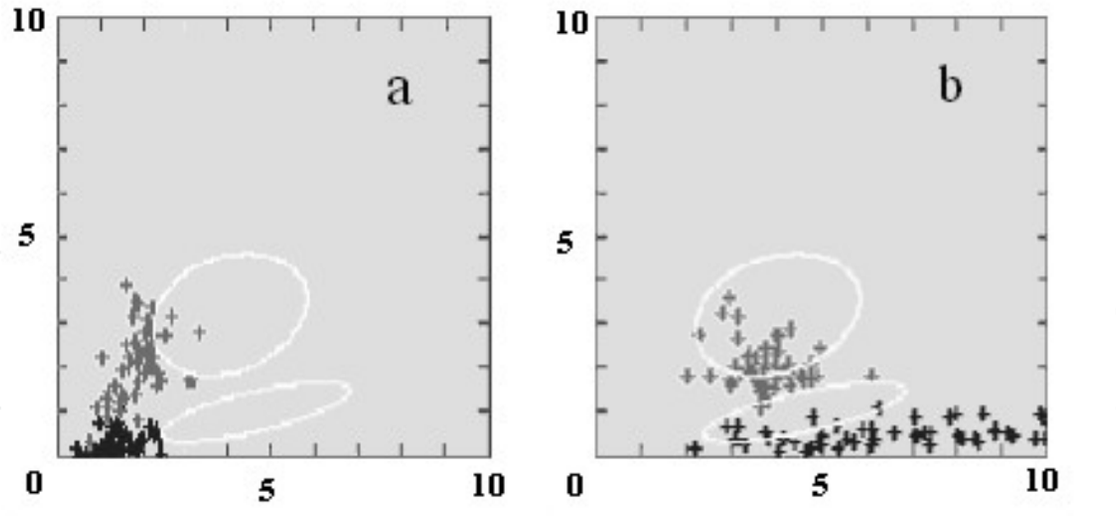

Figure 8. Dual-wavelength microfluorimetry analysis (abscissa and ordinate represent the luminescent intensity I_{530} and I_{640} respectively) of blood immunocytes of oncologic patient (second stage breast cancer). The state before (a) and after (b) the water treatment course (see the text). The black and grey pluses represent lymphocytes and leukocytes respectively. The white ellipses mark the distribution of fluorescent signals of lymphocytes (lower ellipse) and leukocytes (upper ellipse) in norm.

http://dx.doi.org/10.5772/55548

3.2. Biocompatibility of titanium alloys and stainless steel processed in GDP

Stainless steel, titanium and its alloys are among the most utilized biomaterials and are still the materials of choice for many structural implantable device applications [24, 25]. We processed both the titanium and stainless steel samples and investigated changing in their properties caused by GDP.

Current titanium implants face long-term failure problems due to poor bonding to juxtaposed bone, severe stress shielding and generation of debris that may lead to bone cell death and perhaps eventual necrotic bone [26–28]. Improving the bioactivity of titanium implants, especially with respect to cells, is a major concern in the near and intermediate future. Surface properties such as wettability, chemical composition and topography govern the biocompatibility of titanium. Conventionally processed titanium currently used in the orthopedic and dental applications exhibits a micro-rough surface and is smooth at the nanoscale. Surface smoothness on the nanoscale has been shown to favor fibrous tissue encapsulation [27–29]. An approach to design the next-generation of implants has recently focused on creating unique nanotopography (or roughness) on the implant surface, considering that natural bone consists of nanostructured materials like collagen and hydroxyapatite. Some researchers have achieved nano-roughness in titanium substrates by compacting small (nanometer) constituent particles and/or fibers [30]. However, nanometer metal particles can be expensive and unsafe to fabricate. For this reason, alternative methods of titanium surface treatment are desirable.

For the investigation of biocompatibility of implanted materials the tests *in vitro* with the cultures of different cells (fibroblasts, lymphocytes, macrophages, epithelial cells, *etc.*) are used. The influence of material is typically evaluated according to such indicators as adhesion, change in the morphological properties, inhibition of an increase in the cellular population, oppression of metabolic activity and others.

The adhesion of cells, as is known, plays exceptionally important role in the biological processes, such as formation of tissues and organs during embryogenesis, reparative processes, immune and inflammatory reactions, *etc*. Capability for movement is the characteristic property of fibroblasts, cells of immune system and cells, which participate in the inflammation. Moreover, in immunocytes and leukocytes it consists not only in the free recirculation in the blood stream or lymph but also in the penetration into vascular walls and active migration into the surrounding tissues. Adhesion and flattening of cells to the base layer always precede their locomotion. The degree of flattening is important preparatory step to the cell amoeboid mobility. We concentrate our attention on the above components in experiments with titanium alloys.

Titanium samples were cut into pieces (1 cm × 0.5 cm) and placed in a specially constructed plasma generator. They were exposed to glow discharge plasma by ions of the residual gases of the vacuum. The ion energy depended on the voltage in the plasmatron and did not exceed 1–10 keV. Irradiated fluence was 10^{17} ion•cm^{-2}. The temperature of the specimens was controlled during the irradiation process and did not exceed 343 K while the irradiation time varied from 5 to 60 minutes. Rutherford Backscattering Spectrometry (RBS) was used to study the changes after the irradiation. Cell adhesion to titanium samples was tested with L929 mouse connective tissue (fibroblasts-like cells). L929 cells were cultured in Dulbecco's modified Eagle's

medium with 10% fetal bovine serum. Initial cell density was $5 \bullet 10^5$ cells/ml. The samples were placed into the sterile disposable 9 cm diameter tissue culture Petri dishes. 2 ml growth medium with cells were distributed into each Petri then incubated in the 5% CO_2 at 37º C for 2 hours. After that period, cultures were prepared for scanning electron microscopy (SEM).

RBS data for the irradiated sample show the presence of iron on the surface that occurred from high-carbon steel cathode as a result of secondary emission process (Figure. 9). Percentage of iron and thickness of the layer were calculated using RUMP, the program for simulation and analysis based on RBS and Elastic Recoil Detection techniques.

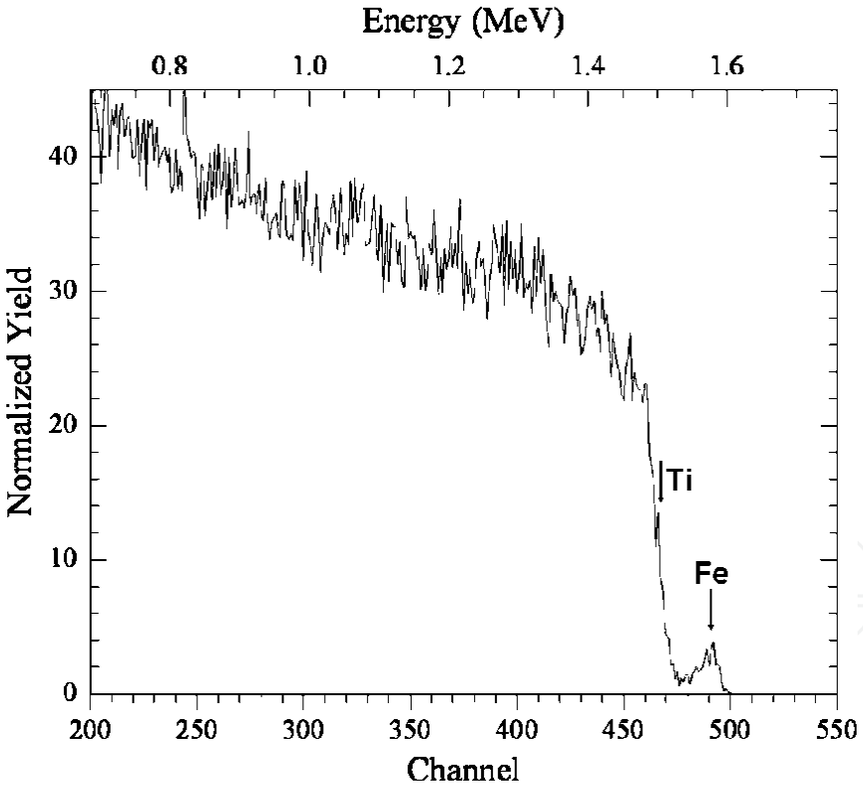

Figure 9. RBS spectrum of the titanium sample irradiated for 5 min at 10 kV.

http://dx.doi.org/10.5772/55548

The obtained data for different voltage and time of the irradiation are presented in Table 2.

Voltage, kV	Time of irradiation, min	Fe:Ti atomic ratio	Density of flattened cells per μm²	Percentage of flattened cells	Increase factor in amount of all cells in comparison with control sample
0.4	60	0.0277:1	534±20	50.2±2.0	1.78
1.2	30	0.0560:1	413±9	43.7±0.9	1.63
10	5	0.0549:1	381±15	42.5±1.7	1.53
Control	0	0:1	26±8	4.4±1.5	1

Table 2. Data obtained from the experiments with titanium samples exposed to GDP.

Calculated data indicate an increase in the density of flattened cells as well as in the cell amount in comparison with the control sample. According to Table 2 one conclude that best adhesion (column 4) and most prolific cell attachment (column 5) correspond to the samples that were exposed to GDP for maximum time at minimum voltage. For this sample we observed less percentage of iron and thickness of the iron layer in comparison with others that were exposed to higher voltage plasma irradiation.

Figure 10 demonstrates SEM images of control and irradiated samples. In comparison with the control sample, analysis of cell attachment for the irradiated samples shows high confluence (attachment ratio) and better spreading.

We also performed experiments on the adhesion of immune-competent cells of human blood to the stainless steel samples. Figure 11 represents the microphotography of the healthy person lymphocytes and leukocytes adhered to the irradiated and non-irradiated plates. As can be seen from photographs, cells, which are located on the different samples, are essentially different. The morphology of leukocytes and lymphocytes, which were adhered to the irradiated material, indicates the expressed amoeboid mobility.

In the majority of the cases endoprosthetics is conducted not in the healthiest people. This fact is very important and it must be considered. Figure 12 displays the results of similar study of the blood nucleus of person who suffers from second stage hypertonia, coronary artery disease and atherosclerosis. From the above data one can conclude that the nature of adhesion of cells to the base layer depends on both the physico-chemical state of this base layer and the state of organism, the owner of cells.

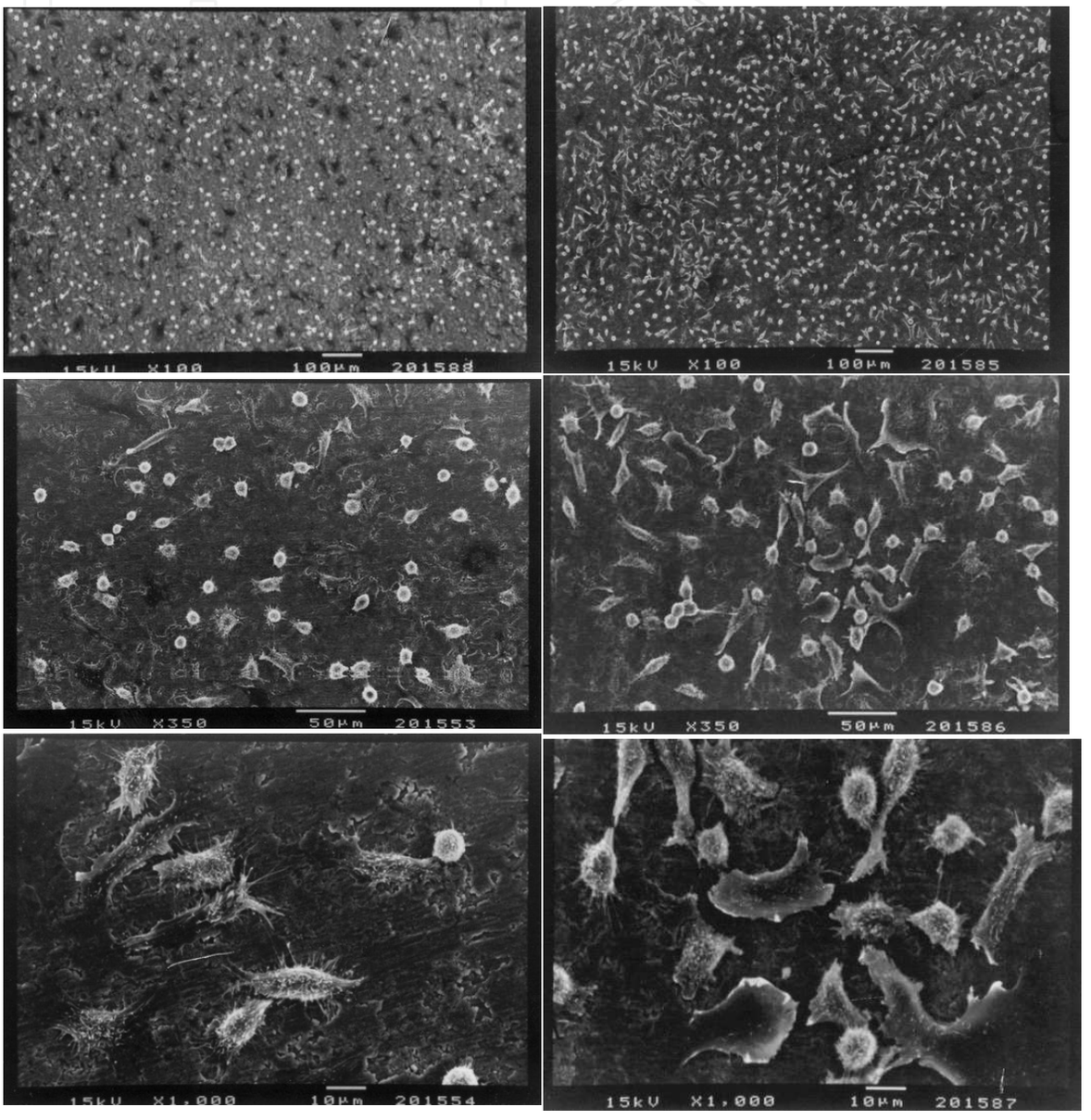

Figure 10. SEM images of cell attachment on (a) the control sample and (b) the titanium sample that was irradiated for 5 min at 10 kV.

http://dx.doi.org/10.5772/55548

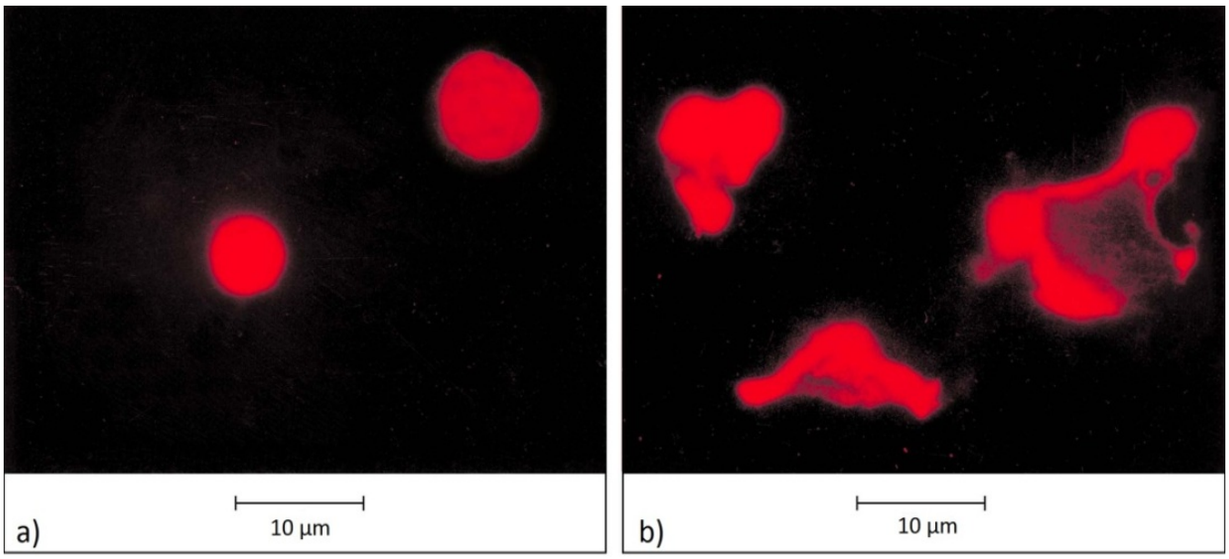

Figure 11. Luminescent microscopy (1000×) of lymphocytes and granulocytes of the blood of healthy donor adhered to (a) non-irradiated and (b) irradiated in GDP surface of the stainless steel samples. The cell nucleus fluorochromization is performed by propidium iodide (λ_{fl} = 615 nm).

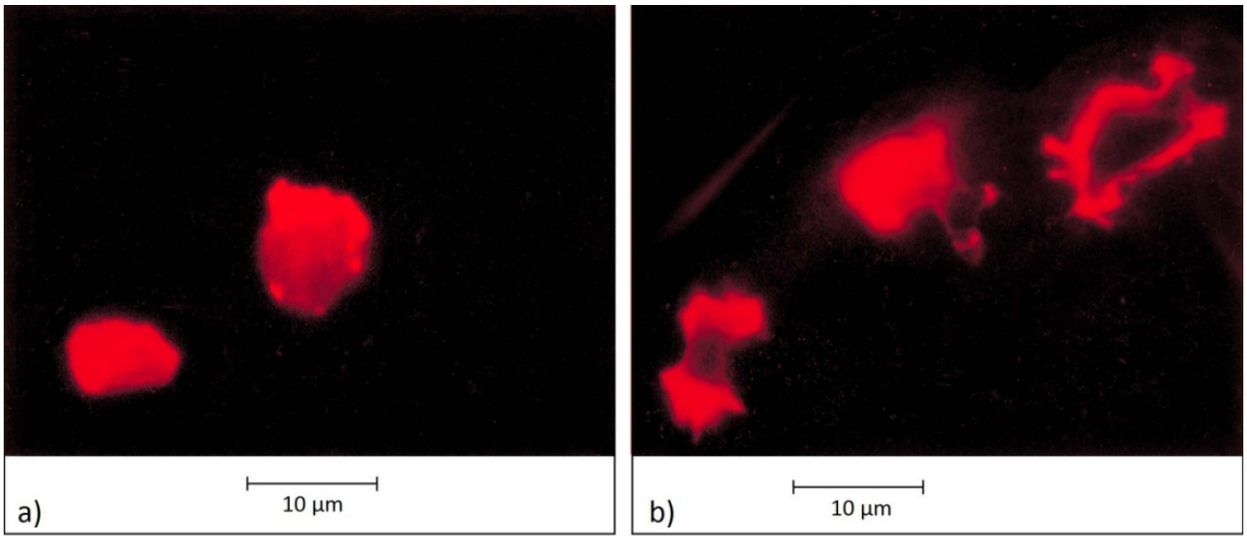

Figure 12. Luminescent microscopy (1000×) *of* lymphocytes and granulocytes of the blood of donor suffering from second stage hypertonia, coronary artery disease and atherosclerosis. The cell nuclei are adhered to (a) non-irradiated and (b) irradiated in GDP surface of the stainless steel samples. The fluorochromization is performed by propidium iodide (λ_{fl} = 615 nm).

4. Discussion and conclusions

Studying the homogeneous chains, like the hydrogen atom chain, exposed to low energies we observed clusterization. It is important to stress that this is truly self-organization phenomenon induced by an external excitation. The chains utilize the excitation energy to initialize nonlinear oscillations and redistribute the energy throughout the chain, which leads to the pattern formation. In the case of multiple impacts on randomly chosen atoms (so-called plasma processing) the atom displacements are by an order higher than in the case of single impact. Thus, the plasma treatment leads to more active self-organization processes and atom rearrangements.

In the cases of inhomogeneous chains containing H and O atoms another type of structures is developed. The shrinkage of chains is so significant that we can say about the collapsed structures. This collapse is observed irrespective of the choice of the atom interaction potentials, whereas the collapsed chain patterns are found to depend on the latter.

To conclude, the performed simulations demonstrated that the system nonlinearity is, in fact, the main reason for the development of self-organization processes leading to significant modifications even in case of low-energy impacts.

In experiments with water and biological objects processed in GDP significant biotrophic effects were detected. The crop seeds and yeast processed directly or indirectly (being immersed in the water processed in GDP) showed markedly greater metabolic activity compared to the control samples. Using the water and the physiological solutions processed in GDP we observed significant therapeutic effects in the test treatments of cardiovascular, oncologic and other diseases. The obtained results suggest the use of discovered phenomena for direct corrections of pathological states by shifting a body state towards its homeostasis. Understanding the mechanisms of the latter will be our next priority.

Next part of this study is devoted to experiments with the titanium alloys and stainless steel exposed to GDP. The experiments with titanium samples reveal an increase in the density of flattened (to the sample surface) cells as well as in the cell amount in comparison with the control sample. These are nothing but preparatory step to the cell amoeboid mobility. Indeed, adhesion and flattening of cells to the base layer always precede their locomotion. According to the results, best adhesion and most prolific cell attachment correspond to the samples that were exposed to GDP for maximum time at minimum voltage. Similar results were obtained in the experiments with stainless steel samples: the morphology of leukocytes and lymphocytes, which were adhered to the irradiated material, indicated the expressed amoeboid mobility. The results with the blood nucleus of person who suffers from several diseases revealed some deviations in the morphology of adhered cells compared to the healthy blood. Thus, the nature of adhesion of cells to the base layer depends on both the physico-chemical state of this base layer and the state of organism, the owner of cells. This circumstance determines even more stringent requirements for the material of the implants.

http://dx.doi.org/10.5772/55548

Author details

V. Tereshko[1*], A. Gorchakov[2], I. Tereshko[3], V. Abidzina[3] and V. Red'ko[4]

*Address all correspondence to: valery.tereshko@uws.ac.uk

1 School of Computing, University of the West of Scotland, Paisley, UK

2 MISTEM, Mogilev, Belarus

3 Department of Physics, Belarusian-Russian University, Mogilev, Belarus

4 Department of Physical Methods of Control, Belarusian-Russian University, Mogilev, Belarus

References

[1] Ziegler, J. F, Biersack, J. P, & Littmark, U. The Stopping and Range of Ions in Solids. New York: Pergamon; (1985).

[2] Eckstein, W. Computer Simulation of Ion-Solids Interaction. Berlin: Springer; (1991).

[3] Tereshko, I. V, Khodyrev, V. I, Tereshko, V. M, Lipsky, E. A, Goncharenya, A. V, & Ofori-sey, S. Self-organizing processes in metals by low-energy ion beams. Nucl. Instr. and Meth. B (1993). , 80, 115-119.

[4] Tereshko, I. V, Khodyrev, V. I, Lipsky, E. A, Goncharenya, A. V, & Tereshko, A. M. Materials modification by low-energy ion irradiation. Nucl. Instr. and Meth. B (1997). , 128, 861-864.

[5] Tereshko, I. V, Glushchenko, V. V, & Tereshko, A. M. Computer simulation of the defect structure formation in crystal lattices by low-energy ion irradiation. Comput. Mater. Sci. (2002). , 24, 139-143.

[6] Tereshko, I, Abidzina, V, Tereshko, A, & Elkin, I. Nanostructural evolution of steel and titanium alloys exposed to glow discharge plasma. Nucl. Instr. and Meth. B (2007). , 261, 678-681.

[7] Tereshko, I. V, Abidzina, V. V, Elkin, I. E, Tereshko, A. M, Glushchenko, V. V, & Stoye, S. Formation of nanostructures in metals by low-energy ion irradiation. Surf. & Coat. Tech. (2007). , 201, 8552-8556.

[8] Stillinger, F. N. Water revisited. Science (1980). , 209(4455), 451-457.

[9] Liu, K, Cruzan, J. D, & Saykally, R. J. Water clusters. Science (1996). , 271(5251), 929-933.

[10] Keutsch, F. N, & Saykally, R. J. Water clusters: untangling the mysteries of the liquid, one molecule at a time. PNAS (2001). , 98(19), 10533-10540.

[11] Galamba, N. Cabral BJC. The changing hydrogen-bond network of water from the bulk to the surface of a cluster: a Born-Oppenheimer molecular dynamics study. J. Am. Chem. Soc. (2008). , 130, 17955-17960.

[12] Luck, W. A. The importance of cooperativity for the properties of liquid water. J. Mol. Struct. (1998).

[13] Shelton, D. P. Collective molecular rotation in water and other simple liquids. Chem. Phys. Lett. (2000).

[14] Lobyshev, V. I, Shikhlinskaya, R. E, & Ryzhikov, B. D. Experimental evidence for intrinsic luminescence of water. J. Mol. Liquids (1999).

[15] Park, J. B, & Lakes, R. S. Biomaterials: An Introduction. New York: Plenum; (1992).

[16] Ratner, B. D, Hoffman, A. S, Schoen, F. J, & Lemons, J. E. editors. Biomaterials Science: Introduction to Materials in Medicine. New York: Academic; (1996).

[17] Abidzina, V, Deliloglu-gurhan, I, Ozdal-kurt, F, Sen, B. H, Tereshko, I, Elkin, I, Budak, S, Muntele, C, & Ila, D. Cell adhesion study of the titanium alloys exposed to glow discharge. Nucl. Instr. and Meth. B. (2007). , 261, 624-626.

[18] Mandl, S, & Rauschenbach, B. Improving the biocompatibility of medical implants with plasma immersion ion implantation. Surf. Coat. Technol. (2002).

[19] Lopez-heredia, M. A, Legeay, G, Gaillard, C, & Layrolle, P. Radio frequency plasma treatments on titanium for enhancement of bioactivity. Acta biomater. (2008). , 4, 1953-1962.

[20] Blank, M, & Goodman, R. Stimulation of stress response by low frequency electromagnetic fields: possibility of direct interaction with DNA. IEEE Trans. Plasma Sci. (2000). , 28, 168-172.

[21] Binhi, V. N, & Savin, A. V. Effects of weak magnetic fields on biological systems: physical aspects. Physics- Uspekhi (2003). , 46(3), 259-291.

[22] Betskii, O. V, Devyatkov, N. D, & Kislov, V. V. Low intensity millimeter waves in medicine and biology. Crit. Rev. Biomed. Eng. (2000).

[23] Gorchakov, A. M, & Karnaukhov, V. N. Melenets YuV, and Gorchakova FT. Identification of pathological conditions by luminescence analysis of immunocompetent blood cells. Biophysics (1999). , 44(3), 550-555.

[24] Hermawan, H, & Ramdan, D. Djuansjah JRP. Metals for biomedical applications. In: Fazel R, editor. Biomedical Engineering- From Theory to Applications. Rijeka: InTech; (2011). , 411-430.

[25] Williams, D. F. Titanium for medical applications. In: Brunette DM, Tengvall P, Textor M, Thomsen P, editors. Titanium in Medicine. Berlin: Springer; (2001). , 13-24.

[26] Buser, D, Nydegger, T, Oxland, T, Cochran, D. L, Schenk, R. K, Hirt, H. P, Snétivy, D, & Nolte, L. P. Interface shear strength of titanium implants with a sandblasted and acid-etched surface: a biomechanical study in the maxilla of miniature pigs. J. Biomed. Mater. Res. (1999). , 45(2), 75-83.

[27] Kaplan, F. S, Hayes, W. C, Keaveny, T. M, Boskey, A, & Einhorn, T. A. Biomaterials. In: Simon SP, editor. Orthopedic Basic Science. Columbus: American Academy of Orthopedic Surgeons; (1994). , 460-478.

[28] Kaplan, F. S, Hayes, W. C, Keaveny, T. M, Boskey, A, Einhorn, T. A, & Iannotti, J. P. Form and function of bone. In: Simon SP, editor. Orthopedic Basic Science. Columbus: American Academy of Orthopedic Surgeons; (1994). , 127-185.

[29] Boyan, B. D, Dean, D. D, Lohmann, C. H, Cochran, D. L, Sylvia, V. L, & Schwartz, Z. The titanium-bone cell interface in vitro: the role of the surface in promoting osteointegration. In: Brunette DM, Tengvall P, Textor M, Thomsen P, editors. Titanium in Medicine. Berlin: Springer; (2001). , 561-586.

[30] Webster, T. J, & Ejiofor, J. U. Increased osteoblast adhesion on nanophase metals: Ti, Ti6Al4V, and CoCrMo. Biomaterials (2004). , 25, 4731-4739.

IntechOpen